Journal of The Electrochemical Society, **160** (10) A1675-A1683 (2013)
0013-4651/2013/160(10)/A1675/9/$31.00 © The Electrochemical Society

Efficient Reformulation of Solid Phase Diffusion in Electrochemical-Mechanical Coupled Models for Lithium-Ion Batteries: Effect of Intercalation Induced Stresses

Sumitava De,[a] Bharatkumar Suthar,[a,*] Derek Rife,[a] Godfrey Sikha,[b,] and Venkat R. Subramanian[a,**,z]**

[a]*Department of Energy, Environmental and Chemical Engineering, Washington University, St. Louis, Missouri 63130, USA*
[b]*Applied Materials Inc, Santa Clara, California 95054, USA*

Lithium-ion batteries are typically modeled using porous electrode theory coupled with various transport and reaction mechanisms with an appropriate discretization or approximation for the solid phase diffusion within the electrode particle. One of the major difficulties in simulating Li-ion battery models is the need for simulating solid-phase diffusion in the second radial dimension *r* within the particle. It increases the complexity of the model as well as the computation time/cost to a great extent. This is particularly true for the inclusion of pressure induced diffusion inside particles experiencing volume change. A computationally efficient representation for solid-phase diffusion is discussed in this paper. The operating condition has a significant effect on the validity, accuracy, and efficiency of various approximations for the solid-phase transport governed by pressure induced diffusion. This paper introduces efficient methods for solid phase reformulation – (1) parabolic profile approach and (2) a mixed order finite difference method for approximating/representing solid-phase concentration variations within the active materials of porous electrodes for macroscopic models for lithium-ion batteries.
 [DOI: 10.1149/2.024310jes]

Manuscript submitted June 11, 2013; revised manuscript received July 12, 2013. Published August 6, 2013.

Electrochemical power sources are expected to play a vital role in the future in automobiles, power storage, military, mobile, and space applications. Lithium-ion chemistry has been identified as a good candidate for high-power/high-energy secondary batteries. Progress has been made toward modeling and understanding of lithium-ion batteries using physics based first principles models which typically solve electrolyte concentration, electrolyte potential, solid-state potential and solid-state concentration in the porous electrodes[1,2] as well as electrolyte concentration and electrolyte potential in the separator. These models are represented by coupled nonlinear partial differential equations (PDEs) in 1-2 dimensions, include physics such as transport phenomena, electrochemistry and thermodynamics and are typically solved numerically which require few minutes to hours to simulate depending on the solver and schemes used.

Currently, silicon, germanium etc. are being pursued as potential anode materials for lithium-ion batteries owing to their high gravimetric (mAh/g) and volumetric capacities (mAh/L) compared to graphite, for high energy and high power applications of the future.[3] During intercalation/de-intercalation these materials exhibit significant stress development as well as volume and density changes.[2,4–6] The concentration gradient inside the particle is affected due to the stress generated within the particle and cannot be captured solely by simple Fickian diffusion. Therefore, pressure induced diffusion must be included when solving for solid phase diffusion in the pseudo radial dimension *r* within the particle.[2,4–6] One of the major difficulties in the electrochemical engineering models is the inclusion of solid phase diffusion in a second dimension *r* which increases the complexity of the model as well as the computation time/cost to a great extent. The inclusion of pressure induced solid phase diffusion physics not only increases the complexity of the model but significantly increases the computational cost/time as it increases the number of equations to be solved in the pseudo *r* dimension. For every point in *x* for the macro-scale, pressure induced solid phase equations have to be solved in *r* and the number of equations depends on the discretization scheme chosen for the *r* dimension. Traditional discretization approaches, such as finite difference (FD), when used in the second pseudo dimension *r* increase the number of equations by many folds thereby making simulation of the system slower and complex.

This paper presents a method for computationally efficient representation of pressure induced diffusion in the solid phase. The paper discusses briefly about the model used for the study of pressure induced diffusion within the electrode particle and the simulation procedure adopted. Then, two computationally efficient representations for pressure induced solid phase diffusion are discussed. At first, a reformulation method is discussed based on the parabolic profile approximation for solid phase diffusion[7] which approximately captures the behavior for low rates and long times. Then, a robust solid phase reformulation technique based on a mixed order finite difference (MFD) method with optimal node spacing is introduced.[8] Results from the parabolic profile approximation are compared with results from the converged solution with 45 internal node points (referred to as full order numerical solution in this manuscript). Results from the MFD technique are also compared with the full-order finite difference solutions for both galvanostatic charging conditions and for current varying as a function of time which suggest that reformulation can be done without compromising on accuracy for a wide range of operating conditions.

Pressure Induced Diffusion within the Electrode Particle

Model equations and boundary conditions.— This paper deals with a one dimensional (1D) continuum scale model that includes pressure induced diffusion in a spherical particle and predicts the stress distribution and volume expansion during charging. This is an important phenomenon to study especially for high capacity electrode materials because during lithium insertion volume expansion of the particle results in strain differential between the inner and outer regions which increases the rate of insertion and therefore develops stress within the particle. This model has been presented in details in Christensen et al.[4] The model accounts for lithium transport, solid mechanics, lithium transport-induced stresses, and volume expansion. Next the model equations and boundary conditions in non-dimensionalized form are briefly reviewed.[4]

For the model, the electrode material is treated as a binary system i.e. a host material occupied with lithium (*LiS*) and pure host material (*S*). Table I presents the dimensionless independent and dependent variables in the system along with their definitions. The equations and boundary conditions for the model were non-dimensionalized accordingly and are presented in Table II. Therefore, there are 8 spatial and time dependent variables along with the moving boundary, $\chi(\tau)$ (particle radius).

*Electrochemical Society Student Member.
**Electrochemical Society Active Member.
zE-mail: vsubramanian@seas.wustl.edu

Table I. List of dimensionless independent and dependent variables for the model.

Independent Variables	Definition
τ	Dimensionless time
ξ	Dimensionless radial distance w.r.t. moving boundary
Dependent Variables	**Definition**
$x_{LiS}\,(\xi, \tau)$	Mole fraction of species *LiS*,
$u\,(\xi, \tau)$	Lattice displacement
$N_{LiS}\,(\xi, \tau)$	Flux of species *LiS*
$N_S\,(\xi, \tau)$	Flux of species *S*
$\theta\,(\xi, \tau)$	Total concentration
$\sigma_r\,(\xi, \tau)$	Stress in radial direction
$\sigma_t\,(\xi, \tau)$	Stress in tangential direction
$\pi\,(\xi, \tau)$	Thermodynamic pressure
$w\,(\xi, \tau)$	Dummy variable used to simplify the equations
$\chi\,(\tau)$	Particle radius

Numerical discretization and simulation.— The system of governing equations and boundary conditions generates a set of highly coupled and non-linear equations. A total of 45 internal node points in the radial direction r were used to achieve a converged solution consistent with the simulation results reported earlier by Christensen et al.[4] An absolute error of 10^{-10} was set for the numerical integration accuracy in time. The simulations were terminated as the surface *LiS* mole fraction reached the maximum value of $x_{\max}$. The set of dimensionless parameters used for simulation is given in Table III. The dimensionless total current I for galvanostatic conditions is calculated based on the C rate and $x_{\max}$. Simulations for both high and low rates and time varying currents were performed.

Table III. Dimensionless parameters used for simulation.

Dimensionless Parameter	Value
ω, fractional expansivity	0.08
e, elatic modulus	399.5
M_b, molar mass ratio	1.09362
$x_{\max}$, maximum mole fraction for lithiation	0.6
D, ratio of diffusive to elastic energy	$8.09e-23$

When converted to finite difference form, the number of equations equals $N_{\text{var}}\,(N+2)+1$ where N_{var} is the number of variables in the system and N is the number of internal node points in r. The time dependent moving boundary provides an additional ordinary differential equation (ODE). For example, when $N=1$ internal node point is used in r, it results in 25 differential algebraic equations (DAEs) of which 4 are of index 2. Higher index DAEs are difficult to solve compared to pure ODEs and DAEs of index 1.[9] Using adaptive

Table II. Model equations and boundary conditions in dimensionless form.

Sr. No	$\xi = 0$	$0 < \xi < 1$	$\xi = 1$	Comments
1	$N_{LiS}\,(\xi, \tau) = 0$	$\frac{\partial}{\partial\tau}(\theta(\xi,\tau)x_{LiS}(\xi,\tau)) - \xi\left(\frac{d}{d\tau}\chi(\tau)\right)\frac{\partial}{\partial\xi}(\theta(\xi,\tau)x_{LiS}(\xi,\tau)) + \frac{\frac{\partial}{\partial\xi}\left(\xi^2 N_{LiS}(\xi,\tau)\right)}{\chi(\tau)\xi^2} = 0$		Mass balance for species *LiS* and *S*
2	$N_S\,(\xi, \tau) = 0$	$\frac{\partial}{\partial\tau}(\theta(\xi,\tau)(1-x_{LiS}(\xi,\tau))) - \xi\left(\frac{d}{d\tau}\chi(\tau)\right)\frac{\partial}{\partial\xi}(\theta(\xi,\tau)(1-x_{LiS}(\xi,\tau))) + \frac{\frac{\partial}{\partial\xi}\left(\xi^2 N_S(\xi,\tau)\right)}{\chi(\tau)\xi^2} = 0$		
3	$N_{LiS}(\xi,\tau) = x_{LiS}(\xi,\tau)(N_{LiS}(\xi,\tau)+N_S(\xi,\tau)) - \frac{\theta(\xi,\tau)}{\chi(\tau)}\left(\alpha\frac{\partial}{\partial\xi}x_{LiS}\,(\xi,\tau) + ex_{LiS}\,(\xi,\tau)\left(1+\frac{\omega}{x_{\max}} - \frac{M_b}{\theta(\xi,\tau)(x_{LiS}(\xi,\tau)M_b+1-x_{LiS}(\xi,\tau))}\right)\frac{\partial}{\partial\xi}\pi(\xi,\tau)\right)$	$\chi\,(\tau)^2\left(N_{LiS}\,(\xi,\tau) - \theta\,(\xi,\tau)\,x_{LiS}\,(\xi,\tau)\,\frac{d}{d\tau}\chi\,(\tau)\right) = -I$		Stefan-Maxwell equation for flux of *LiS*. The surface current flux condition is used at $\xi = 1$.
4	$\theta\,(\xi,\tau) = \left(1+\frac{\omega x_{LiS}(\xi,\tau)}{x_{\max}}\right)^{-1}\left(e^{\frac{\sigma_r(\xi,\tau)+2\sigma_t(\xi,\tau)-3\pi(\xi,\tau)}{1+\nu}}\right)^{-1}$			Total concentration of species as a function of of mole fractions and stresses
5	$u\,(\xi,\tau) = 0$	$\frac{N_{LiS}(\xi,\tau)+N_S(\xi,\tau)}{\theta(\xi,\tau)} = \frac{\frac{\partial}{\partial\tau}u(\xi,\tau) - w(\xi,\tau) - \xi\frac{d}{d\tau}\chi(\tau)}{1-w(\xi,\tau)}$	$\frac{N_{LiS}(\xi,\tau)+N_S(\xi,\tau)}{\theta(\xi,\tau)} = \frac{\partial}{\partial\tau}u(\xi,\tau)$	The relationship between the total flux of the species and radial displacement
6	$\sigma_r\,(\xi,\tau) = w\,(\xi,\tau) - \frac{w(\xi,\tau)^2}{2}$	$\sigma_r\,(\xi,\tau) = (1-\nu)\left(w(\xi,\tau) - 1/2(w(\xi,\tau))^2\right) + 2\nu\left(\frac{u(\xi,\tau)}{\xi\chi(\tau)} - 1/2\frac{(u(\xi,\tau))^2}{\xi^2(\chi(\tau))^2}\right)$		Hooke's Law for radial and tangential stresses. At center, both are equal.
7	$\sigma_t\,(\xi,\tau) = w\,(\xi,\tau) - \frac{w(\xi,\tau)^2}{2}$	$\sigma_t\,(\xi,\tau) = \nu\left(w(\xi,\tau) - 1/2(w(\xi,\tau))^2\right) + \frac{u(\xi,\tau)}{\xi\chi(\tau)} - 1/2\frac{(u(\xi,\tau))^2}{\xi^2(\chi(\tau))^2}$		
8	$\frac{\partial}{\partial\xi}\pi\,(\xi,\tau) = 0$	$\frac{\partial}{\partial\xi}\left(\sigma_r\,(\xi,\tau) - \pi\,(\xi,\tau)\right) + 2\frac{\sigma_r(\xi,\tau)-\sigma_t(\xi,\tau)}{\xi} = 0$	$\sigma_r\,(\xi,\tau) - \pi\,(\xi,\tau) = 0$	Momentum balance. Existence of free surface at $\xi = 1$.
9	$w\,(\xi,\tau) = \frac{\frac{\partial}{\partial\xi}u(\xi,\tau)}{\chi(\tau)}$			Dummy variable
10	$\frac{d}{d\tau}\chi(\tau) = \frac{\partial}{\partial\tau}u(\xi,\tau)$			Moving boundary

solvers in time gives an advantage in numerical simulation in terms of efficiency, but also requires additional robustness on the choice of DAE solvers. Discussion of the difficulty of index-2 DAEs is beyond the scope of the paper. A future publication will address the optimal way of solving pressure induced diffusion in intercalation electrodes depending on the physics included.

Reformulation of Pressure Induced Solid Phase Diffusion: Parabolic Profile Approximation

A first attempt to approximate the model is to assume a parabolic polynomial profile for spatially dependent variables. In the past,[7,10] this method has shown reasonable accuracy and has been used in the macroscopic P2D battery model.[1] This approximation method for pressure induced solid phase diffusion is based on assuming profiles inside the particle as parabolic in nature and generating volume averaged equations. This method has been discussed for a radial Fickian diffusion equation previously by other authors.[10–12] The following section describes the step by step derivation of the approximate profiles and volume averaged equations based on this method. For demonstration purposes, we choose a representative variable from the model e.g. the flux of species LiS. Therefore, assuming parabolic profile we can write,

$$N_{LiS}(\xi, \tau) = a1_0(\tau) + a1_1(\tau)\xi + a1_2(\tau)\xi^2 \quad [1]$$

All the other spatial variables of the system can be expressed with similar profiles. For the simulation of such a system, we need to solve the time dependent coefficients which appear in the assumed profiles. As a first step, to eliminate one of the coefficients, a volume averaged quantity is introduced into the system. For the demonstration case considered here, $\overline{N}_{LiS}(\tau)$ is the volume averaged flux of species LiS which can be represented by

$$\overline{N}_{LiS}(\tau) = \int_0^1 3\xi^2 (N_{LiS}(\xi, \tau)d\xi \quad [2]$$

Replacing Eq. 1 in Eq. 2 and performing the integration, the time dependent coefficient $a1_2(\tau)$ can be removed in terms of the volume averaged quantity and other coefficients as

$$a1_2(\tau) = \frac{5}{3}\left(\overline{N}_{LiS}(\tau) - \frac{3}{4}a1_1(\tau) - a1_0(\tau)\right) \quad [3]$$

Replacing this value in Eq. 1, the parabolic profile equation for $N_{LiS}(\xi, \tau)$ becomes

$$N_{LiS}(\xi, \tau) = a1_0(\tau) + a1_1(\tau)\xi + \frac{5}{3}\left(\overline{N}_{LiS}(\tau) - \frac{3}{4}a1_1(\tau) - a1_0(\tau)\right)\xi^2 \quad [4]$$

Now there are 2 time dependent coefficients along with the volume averaged quantity. The boundary conditions are to be used for eliminating the time dependent coefficients. Using the boundary condition for $N_{LiS}(\xi, \tau)$ at $\xi = 0$, the coefficient $a1_0(\tau)$ can be eliminated and the parabolic profile can be rewritten as

$$N_{LiS}(\xi, \tau) = a1_1(\tau)\xi + \frac{5}{3}\left(\overline{N}_{LiS}(\tau) - \frac{3}{4}a1_1(\tau)\right)\xi^2 \quad [5]$$

The remaining time dependent coefficient is eliminated by using the boundary condition at $\xi = 1$. It has to be noted that due to the non-linearity and implicit nature of the system, the application of boundary condition at $\xi = 1$ does not generate explicit expressions for the coefficients to be directly incorporated into the parabolic profiles. Therefore, these boundary conditions were solved as a coupled set of equations within the final system. Finally, the volume averaged quantity was evaluated by volume averaging the entire governing equation. In general, this step can be mathematically represented as

$$\int_0^1 3\xi^2 (GE(\xi, \tau))d\xi = 0 \quad [6]$$

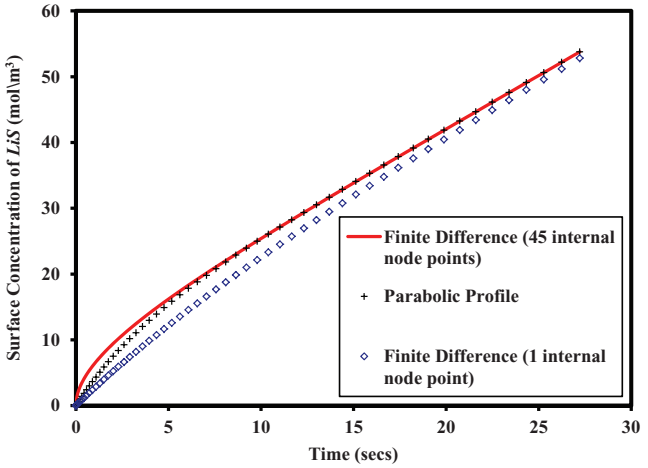

Figure 1. Comparison of parabolic profile method with finite difference numerical solution with 45 and 1 equally spaced internal node points for charging rate of C/3.

where $GE(\xi, \tau)$ is any governing equation of the system. Direct analytical integration was performed in ξ for most of the governing equations except for some (Sr. No. 3, 4 & 5 from Table II). Numerical integration in ξ was performed for these particular equations using Simpson's rule. Simulations were performed with an increasing number of integration points to verify the convergence of the solution. These mathematical steps are performed for all spatially varying quantities to generate the reformulated parabolic profile model for the simulation of pressure induced diffusion within the electrode particle.

The advantage of this method of reformulation is that it reduces the number of state variables thereby reducing number of equations which facilitates faster simulation. This method is accurate for low rates and long times. After the reformulation technique is applied, the equations are only functions of dimensionless time τ and can be solved using time adaptive solvers[9,13–15] with proper initialization. Only certain solvers like Maple's DSOLVE, MEBDFI can handle index 2 DAE systems directly but for commonly used solvers like DASKR,IDA it must be converted to an index 1 system before numerical simulation.

The model for pressure induced diffusion has 8 dependent variables varying spatially and in time (Table I). The moving radius is tracked by $\chi(\tau)$ which is a time dependent variable. Therefore, if discretized with $N = 1$ internal node point (FD method), the total number of states is equal to $(8*3) + 1 = 25$. For the parabolic profile, the general representation of a dependent variable is given by

$$f(\xi, \tau) = f1_0(\tau) + f1_1(\tau)\xi + f1_2(\tau)\xi^2 \quad [7]$$

Therefore, there are three time dependent coefficients per variable which generates $(8*3) = 24$ states for the model discussed in this paper. Taking the moving boundary variable into account, the reformulated parabolic profile pressure induced diffusion model generates 25 state variables before mathematical manipulation which is exactly similar to the case when the original model is discretized with $N = 1$ internal node point. Therefore, it is logical to compare the parabolic profile approximation results with full-order numerical solution of the model discretized using FD method for $N = 1$ internal node point. The dimensional surface concentration $c_{surf}(x, t)$ is the quantity of interest because it is required by the macro-homogeneous battery model to keep track of the local current density as a function of time. Therefore, results for surface concentration are compared in Fig. 1 from the full-order solution and the reformulated model for a C/3 rate. Note that a low rate was chosen for this case as the parabolic profile approximation is likely to be valid only for low rates. The converged numerical solution with $N = 45$ internal node points was chosen as the benchmark for the comparison of the results.

The results of Fig. 1 clearly show that at short times i.e. at the start of lithiation of electrode particle, the parabolic profile

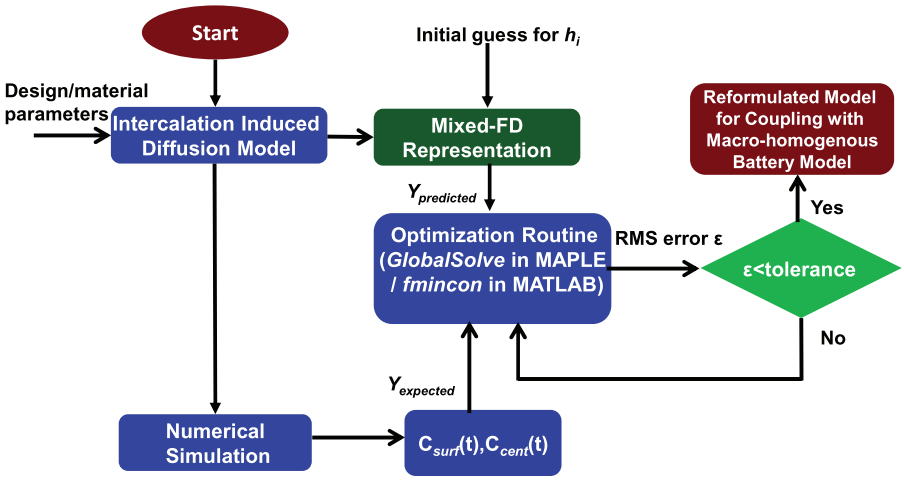

Figure 2. Schematic of steps involved in mixed FD method for optimized node spacing and hence reformulation of pressure induced diffusion in solid-phase. $Y_{predicted}$ and $Y_{expected}$ are the values of the center and surface concentrations as predicted from full order numerical solution and MFD simulation respectively.

approximation predicts erroneous results compared to the numerical solution with $N = 45$ internal nodes. But the parabolic profile predictions become reasonable at longer times. This behavior is observed because the model fails to capture the effect of the moving front depicted by steep concentration gradients at short times when lithiation initiates.[4] As time increases and lithiation continues, the effect of pressure induced diffusion decreases and the parabolic profile predicts surface concentration $c_{surf}(x, t)$ with reasonable accuracy. As expected, the FD simulation with $N = 1$ node point gives erroneous results for both short and long times. Therefore, if we are only concerned about the accuracy of surface concentration at long times and very low rates, then the parabolic profile approximation is a good choice as it has significantly less number of states compared to the FD simulation with 45 internal node points (25 states compared to 477 states) which facilitates a reduction in the computational cost/time. In the next section, the mixed finite difference method with optimal node spacing is introduced which is robust and accurate for both short and long times. Note that volume averaging provides good enough results and conserves mass and charge at long times.

Reformulation of Pressure Induced Solid Phase Diffusion: Mixed Finite Difference Approach with Unequal Node Spacing

Finite difference method is one of the most widely used numerical techniques to solve ordinary and partial differential equations. Use of finite difference method has been the first choice for solving first principles based lithium-ion battery models. However, for macro-micro scale coupled battery models, when dealing with a second radial dimension r for discretization, the number of equations increases by many folds, thereby increasing the computational cost.[8,10,16] As mentioned previously, over 40 internal node points in r are needed to obtain a converged solution for simulation of the model. Use of such a large number of node points in the r direction will increase the number of equations by a great deal and hence, we used a mixed order finite difference approach, wherein we use less number of node points with unequal node spacing. It is to be noted that, the macroscopic battery model requires only the lithium concentration at the surface of the particle, $c_{surf}(x, t)$, as a function of local reaction current density, $j(t)$. For this reformulation method, the node points are chosen optimally. Derivation of finite difference notations for different approximation for the derivatives is given in the following section.[8,17]

Taylor series expansions at $x = x+h_{i+1}$ and $x - h_i$ are written as

$$f(x + h_{i+1}) = f(x) + \left(\frac{d}{dx} f(x)\right) h_{i+1} + \frac{1}{2}\left(\frac{d^2}{dx^2} f(x)\right) {h_{i+1}}^2 \quad [8]$$

$$f(x - h_i) = f(x) - \left(\frac{d}{dx} f(x)\right) h_i + \frac{1}{2}\left(\frac{d^2}{dx^2} f(x)\right) {h_i}^2 \quad [9]$$

where h_i is the unequal node spacing between i^{th} and $(i\text{-}1)^{th}$ nodes in the domain. Truncating the series expansion with the required amount of accuracy and solving for the first and second order derivatives, we can obtain central finite difference formulas for the first and second order derivatives. We use an order of h^2 accuracy for all of our approximations.

$$\left(\frac{dc}{dx}\right)_{central} = \frac{-c_{i+1}{h_i}^2 + c_i{h_i}^2 + {h_{i+1}}^2 c_{i-1} - {h_{i+1}}^2 c_i}{h_{i+1}(h_i + h_{i+1}) h_i} \quad [10]$$

$$\left(\frac{d^2c}{dx^2}\right)_{central} = 2\frac{c_{i+1}h_i - c_i h_i + h_{i+1}c_{i-1} - h_{i+1}c_i}{h_{i+1}(h_i + h_{i+1}) h_i} \quad [11]$$

Similarly forward and backward finite differences relations for the derivatives can be obtained, and used for boundary conditions.

$$\left(\frac{dc}{dx}\right)_{forward} = -\frac{c_{i+2}{h_{i+1}}^2 - {h_{i+1}}^2 c_{i+1} - 2h_{i+1}h_{i+2}c_{i+1} + 2h_{i+1}h_{i+2}c_i - {h_{i+2}}^2 c_{i+1} + {h_{i+2}}^2 c_i}{h_{i+2}(h_{i+1} + h_{i+2}) h_{i+1}} \quad [12]$$

$$\left(\frac{dc}{dx}\right)_{backward} = \frac{c_{i-2}{h_i}^2 - {h_i}^2 c_{i-1} - 2h_i h_{i-1}c_{i-1} + 2h_i h_{i-1}c_i - {h_{i-1}}^2 c_{i-1} + {h_{i-1}}^2 c_i}{h_{i-1}(h_i + h_{i-1}) h_i} \quad [13]$$

Fig. 2 presents a general methodology for obtaining efficient reformulation/representation of the pressure induced solid-phase diffusion equations in the pseudo radial r dimension within the particle.

First, a Mixed-FD representation is written with $N = 5$ internal node points. For the optimization scheme, using $0.001 < h_i < 0.999$ as the constraint, the error between expected full-order numerical solution and the mixed-FD method is minimized to a set tolerance. At first, the optimal node spacing for a lower rate of charge was found (by setting equal node spacing as initial guess). This is done because at low rates only geometry dictates the optimal node spacing (similar to primary current distribution in electrochemical systems). The optimal node spacing from low rates was used as initial guess to predict optimal node spacing for higher rates during which severe mass transfer limitations occur. The optimal node spacing obtained for higher rates was then used as initial guess to predict the best node spacing distribution for time dependent current which is reflective of spatially distributed and highly transient pore wall flux for macro-homogenous battery models. Mathematically, it can be represented

as:

$$\begin{aligned} &\min_{h_i} E \\ &\text{subject to:} \\ &\frac{dy}{dt} = f(y, u, h_i) \\ &g(y, u, h_i) = 0 \\ &0.001 \le h_i \le 0.999 \end{aligned} \qquad [14]$$

Here E is RMS error between full order numerical solution and the reformulated MFD solution, while y and u represent the differential and algebraic states in the model respectively. Numerous methods are available for solving constrained dynamic optimization problems, including (i) variational calculus, (ii) Pontryagin's maximum principle, (iii) control vector iteration, (iv) control vector parameterization, and (v) simultaneous nonlinear programming.[18,19] The control vector parameterization (CVP)[19] is a widely applied method employed in this study, due to its ease of implementation. Typically, Jacobian based methods are sufficient for convergence.[20] For difficult/severe nonlinearities, global optimization techniques including genetic algorithms might be required for convergence and robustness[21,22] though they are likely to be very slow. For performing the multivariable optimization scheme discussed above, the inbuilt gradient based optimization algorithms in Maple's *GlobalSolve* function (Global Optimization Toolbox) were used. Typically computational times for the simulation of optimization schemes range from minutes to hours.

One of the advantages of the MFD method is that, the radial concentration gradient is more significant near the surface compared to the center and hence, strategically placing more node points near the surface and less node points at the center can capture that behavior without increasing the fineness of the mesh everywhere. However, radial stress is maximum at the center of the particle and an optimization scheme is needed to allow for accurate prediction at the center of the particle (as opposed to arbitrarily using a finer mesh near the surface). Lesser node points in r leads to less state variables and equations and hence faster simulation for the whole battery model. The placement of these node points is important and in order to find the exact position of these node points we ran an optimization algorithm to find the best h_1, h_2, h_3, *etc.* and minimize N and the CPU time for efficient coupling with macro-homogenous models. This method is very accurate for short times/high rates/pulses; and is applicable for a wide range of operating conditions. Therefore this approach is very robust.

The model was then simulated with the optimally spaced node points using similar operating conditions and parameters which were used for full order numerical simulation using a DAE solver (DSOLVE/IDA)[13] with consistent initial values. We applied a mixed finite difference optimal node spacing approach for higher rates of galvanostatic charge and also for a time varying current case. For the mixed FD method we used 5 optimally placed internal node points in the pseudo dimension r within the particle and compared the results (dimensional surface concentration $c_{surf}(x, t)$) with full order numerical solution with 45 internal node points in r. To show the efficiency and accuracy of the optimally spaced node point method, we also compared surface concentration results for simulations with 5 equally spaced internal node points in r. We chose high rates of charge, ranging from 2 to 10 C as the concentration gradient within the particle is more prominent for these cases. This makes it difficult to predict the surface concentration accurately with a small number of node points when not placed optimally. Figs. 3 to 6 show the comparisons between the above mentioned cases for 2, 3 5 and 10 C rates respectively. It is to be noted that for all the plots, we compared $c_{surf}(x, t)$ for the first 2 to 3 seconds at the start of lithiation. This is because stress reaches maximum value within the first few seconds of lithiation and then decreases and finally equilibrates with time. The effect of pressure induced diffusion is thus most significant at short times.[4] This effect alters the concentration gradient within the particle significantly. Therefore, it is best

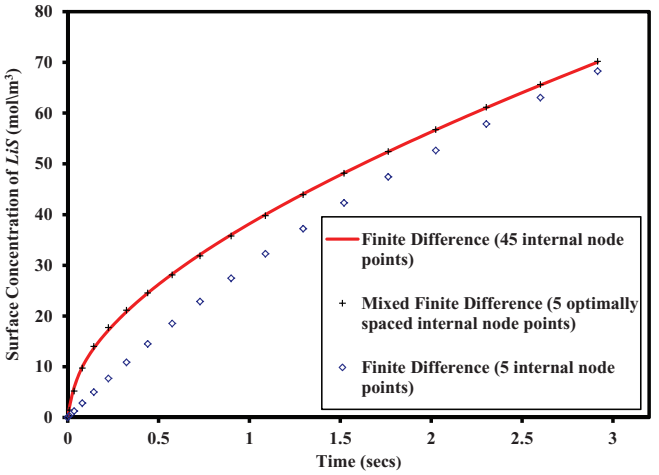

Figure 3. Comparison of mixed finite difference method with 5 optimally placed internal node points with finite difference numerical solution with 45 and 5 equally spaced internal node points for charging rate of 2C.

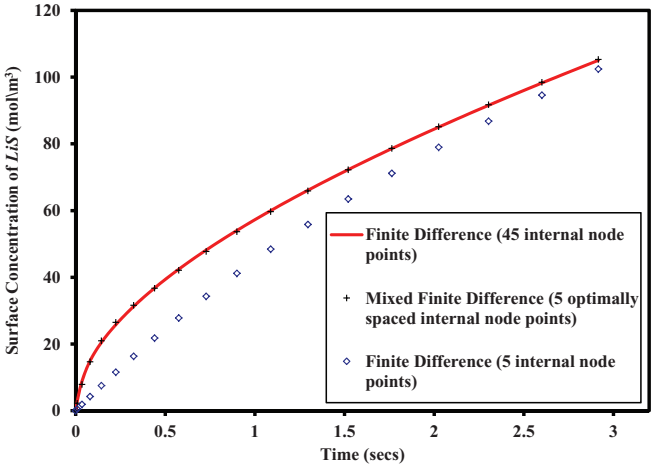

Figure 4. Comparison of mixed finite difference method with 5 optimally placed internal node points with finite difference numerical solution with 45 and 5 equally spaced internal node points for charging rate of 3C.

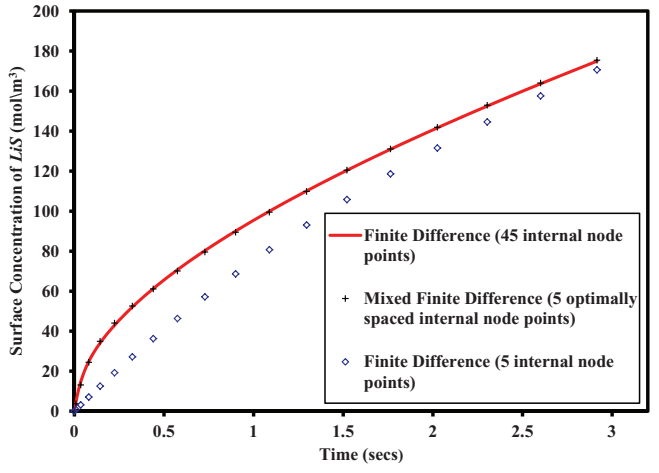

Figure 5. Comparison of mixed finite difference method with 5 optimally placed internal node points with finite difference numerical solution with 45 and 5 equally spaced internal node points for charging rate of 5C.

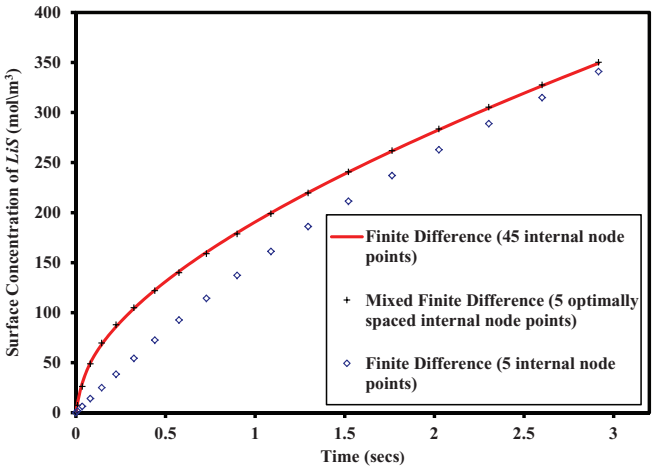

Figure 6. Comparison of mixed finite difference method with 5 optimally placed internal node points with finite difference numerical solution with 45 and 5 equally spaced internal node points for charging rate of 10C.

to compare the results within that time frame because the efficiency and accuracy of the mixed FD model will be more visible compared to equally spaced node point simulation cases. However, the reformulated model is valid for the entire lithiation regime. From the plots it is clear that the MFD reformulated model agrees accurately with the full-order numerical solution. The results from the equal node spacing case for low number of node points are clearly erroneous showing the importance and strategic benefits of placing the points optimally. Table IV presents the values of optimized node spacing obtained in this case for different values of dimensionless current. As expected, the density of optimally placed node points increases along the radial direction r from the center to the surface following the direction of increment of concentration gradient within the particle. The simulation times from the MFD method are compared with the times from full-order numerical solution with 45 internal node points in r in Table V. The simulation times reported here are with respect to a cut-off of maximum lithiation mole fraction of 0.6 at the surface of the particle. The MFD method shows increased computational efficiency compared to full-order numerical solution as shown by the simulation times presented. Although Maple's solver directly solves the index 2 system, the computational times depend on the total time of simulation (robust solvers are expected to be independent of the total time of simulation). Therefore, we see the decrease in simulation times with increase in rates from Table V. The CPU times reported are based on simulations run on a computer using a 3.33 GHz Intel 12 core processor with 24 GB RAM. The compiled version of Maple is 10-20 times faster than the non-compiled version. For larger number of equations, the compiled version of Maple is slower than a typical IDA[13] call for the same number of equations as Maple does not use sparse storage methods for its DAE solvers. As mentioned earlier, the stress model is an index 2 DAE system. As IDA cannot solve index 2 DAE systems directly, the system was converted to a index 1 system to simulate with IDA and compare simulation times with Maple's DSOLVE. For 2 C rate, use of the IDA solver reduced the computation time to around 10 seconds for a full-order numerical solution with 45 internal node

Table IV. Optimized node spacing for different C rates for mixed finite difference reformulation method.

C rate	Optimized node spacing (h_i)
≤ 2	[0.4764,0.1361,0.1699,0.1403,0.0525,0.0264]
3	[0.4762,0.1385,0.1675,0.1427,0.0505,0.0263]
5	[0.4780,0.1405,0.1629,0.1450,0.0491,0.0262]
10	[0.4779,0.1443,0.1582,0.1474,0.0478,0.0262]

Table V. Simulation times for different C rates for mixed finite difference reformulation method and full-order numerical solution with 45 equally spaced internal node points.

C rate	Simulation time for full-order numerical solution (s)	Simulation time for MFD reformulation (s)
≤ 2	1229.272	186.951
3	810.269	130.697
5	451.373	78.920
10	245.593	38.142

points and around 2 seconds for the reformulated FD model with 5 optimally spaced node points. Nevertheless, it is clear that 1-2 orders of magnitude difference in CPU time is observed for the MFD reformulated model compared to the full-order model for the solid phase diffusion. Therefore, one can conclude that the reformulated MFD approach decreases the computational cost, and will play a key role in simulation efficiency when coupled with macroscopic battery models.

Fig. 7 shows the comparison of the mixed FD method, with the traditional finite difference numerical solution with 45 and 5 equally spaced internal node points in r for dimensionless total current I varying with dimensionless time. The current applied is chosen as $I = 1 + \sin(100^*\tau)$. When the flux at the surface varies with time, then it is a real challenge to predict concentration profile accurately with less node points which is evident from the results obtained with 5 equally spaced internal nodes in r. The simulation was stopped when the surface mole fraction of LiS reached $x_{\max}$. From this figure it is clear that results obtained with the full-order numerical solution (45 equally spaced internal node points in r) can be efficiently obtained at reduced computational time with no compromise in accuracy with the mixed FD reformulated model. The optimal node spacing for the MFD simulation was [0.5937,0.1542,0.1058,0.0982,0.0256,0.0224]. The simulation time taken is 18.8 seconds which is significantly less than that for the full-order numerical solution (547.41 seconds). This result shows the robustness of the MFD reformulation approach which can be confidently used for a large set of operating conditions.

For optimizing the node spacing h_i in the radial direction r, the error for the surface concentration $c_{surf}(x, t)$ of species LiS between the expected full-order numerical solution and the mixed-FD method was minimized to a set tolerance. But this approach compromises on the concentration profile at the center of the particle and therefore affects the radial stress profile at center.[2] As radial stress is maximum (tensile stress) at the center during charging, correct prediction

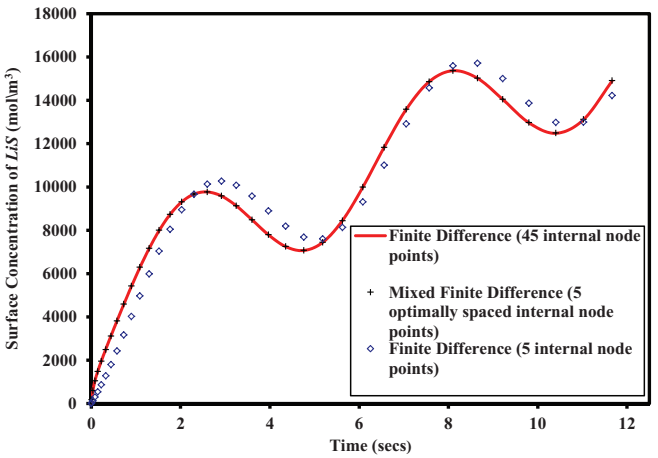

Figure 7. Comparison of mixed finite difference method with 5 optimally placed internal node points with finite difference numerical solution with 45 and 5 equally spaced internal node points for current I varying as a function of time.

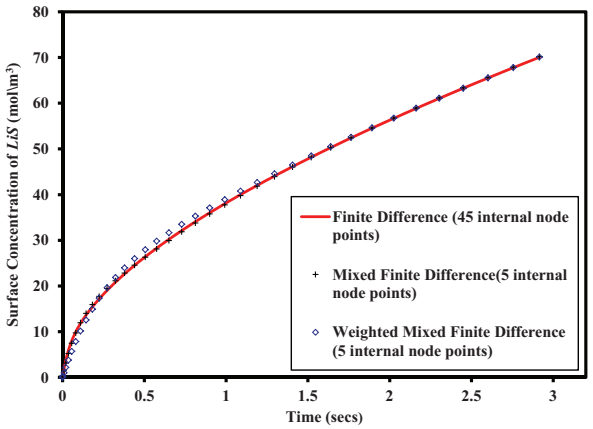

Figure 8. Comparison of surface LiS concentration from the MFD reformulated models and full-order numerical simulation with 45 equally spaced internal node points for charging rate of 2C.

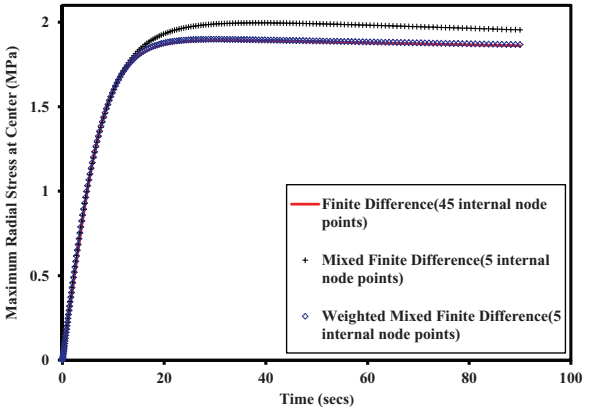

Figure 9. Comparison of maximum radial stress from the MFD reformulated models and full-order numerical simulation with 45 equally spaced internal node points for charging rate of 2C.

of this quantity is important because the magnitude plays a critical role in determining the conditions for the fracture of the particle during lithium insertion. Moreover, for development of micro-macroscale electrochemical- mechanical coupled models for lithium ion batteries, the prediction of maximum radial stress becomes important. Therefore to achieve reasonable predictions for the maximum stresses, the MFD method was modified such that the errors from both the center and surface *LiS* concentrations between expected full-order numerical solution and the mixed-FD method were minimized for optimization of node spacing. It is to be noted that unequal weights were applied to each of the individual errors and the sum of the weighted errors was assigned as the objective function to minimize with similar constraints used earlier for the optimization protocol. 5 internal node points were found to be sufficient for the model chosen. In our opinion, minimizing the error for center concentration can facilitate more accurate predictions for the maximum radial stress. Zhang et al.[2] showed with a slightly different and simpler stress strain modeling approach (strain splitting or thermal analogy modeling) that without consideration of moving boundary and assuming constant density, both the radial and tangential stresses can be explicitly expressed as a function of average concentration and concentration at center and surface of particle. For our system, this relationship is not explicit but as both average (Faraday's law for charge conservation) and surface concentration are accurately predicted by MFD method, maximum tangential stress is always predicted accurately in the MFD approach irrespective of whether both center and surface concentrations or only surface concentration is considered for minimization of error. The maximum radial stress is more difficult to predict with approximate methods as the concentration moves toward the center. This drives our attempt to introduce the new weighted MFD method where errors for both the center and surface concentrations are minimized simultaneously.

Fig. 8 compares the results from the two MFD methods discussed and the full-order numerical solution with 45 internal node points in r for the surface concentration $c_{surf}(x,t)$ for 2C rate of charge. It is clear from the plot, that the weighted error minimization MFD technique compromises on the surface concentration predictions slightly, especially at short times where the concentration profile has a steep gradient. The maximum radial stress profiles at the center of the particle for the MFD techniques are compared with the full-order numerical solution in Fig. 9 for 2C rate. Simulation from the weighted error MFD method predicts the stress values with reasonable accuracy. But simulation results from the MFD method minimizing error for only the surface concentration, shows significant error compared to the full-order numerical solution. Fig. 10 shows the comparison of the maximum tangential stress profiles obtained from the two MFD methods with the full order numerical solution for 2C rate. As discussed earlier, both the MFD methods predict the maximum tangential stress at the surface with reasonable accuracy. The optimal node spacing obtained for the weighted error MFD method simulation was [0.4052,0.0348,0.2825,0.1372,0.1024,0.0391].

Therefore, minimizing errors for both the center and surface concentrations simultaneously to optimize node spacing, leads to errors in the prediction of surface variables as seen from the results. It is to be noted that the weighted error MFD method is a case of multi-objective optimization and minimizing both errors with as low as 5 node points is difficult. This is the reason for which a small compromise in the surface concentration predictions is observed. In our opinion, using higher order finite difference discretization schemes (third or fourth order) or larger number of node points, this error can be remedied, but higher order approximations can induce instability in numerical simulation. As our final aim is to reduce computational cost, obtaining reasonably accurate predictions with minimum number of node points is our priority.

Generality of the Proposed Mixed Finite Difference Approach

The results discussed from both the MFD approaches in the previous section were derived for isotropic graphite as the electrode particle material. At present, for high energy/power applications, novel materials like silicon are emerging as the suitable candidates for state-of-art electrodes. An attempt was made to verify the generality of the MFD approach by using the optimal node spacing obtained for graphite to predict the surface concentration and stress profiles for silicon. Simulations were performed for a spherical particle of silicon of 50 nm

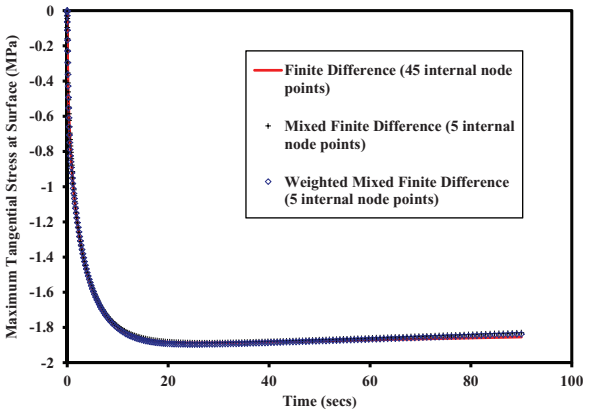

Figure 10. Comparison of maximum tangential stress from the MFD reformulated models and full-order numerical simulation with 45 equally spaced internal node points for charging rate of 2C.

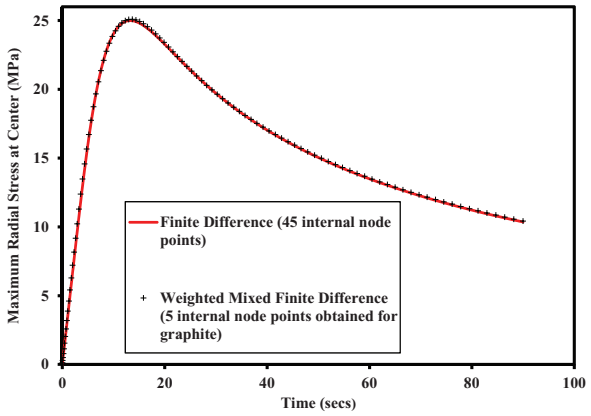

Figure 11. Comparison of maximum radial stress from the weighted MFD reformulated model and full-order numerical simulation with 45 equally spaced internal node points for charging rate of 1C for silicon using optimal node spacing derived for graphite.

radius for a 1 C rate of charge. The optimal node spacing obtained from the weighted MFD method discussed earlier was used to predict the silicon profiles. Fig. 11 and 12 show the comparison of the maximum radial and tangential stress profiles predicted by the weighted MFD approach with the full order numerical solution. It is evident from the plots that the MFD simulation using optimal node spacing corresponding to graphite predicts the stress profiles with reasonable accuracy for silicon. Although it is advisable to derive a separate set of optimal node spacing for a specific material, this study proves the generality and robustness of the proposed MFD approach.

Conclusions

A detailed continuum scale model for pressure induced diffusion during lithiation of an electrode particle was reviewed[4] and the characteristics of the system of equations representing the model and its simulation were discussed. Two efficient reformulation techniques were introduced. The parabolic profile reformulation method was developed based on assuming parabolic profiles for dependent variables in the radial dimension r within the particle and generating volume averaged equations. The mixed finite difference reformulation approach is based on using lesser number of optimally spaced node points in radial dimension r within the particle. Both of the methods reduce the number of states compared to full-order numerical solution using large number of node points and therefore reduce computational cost/time. The parabolic profile reformulation method is accurate for low rates and long times. The mixed finite difference approach is an accurate and robust method for low/high rates, short/long times and can be used with confidence for a wide range of operating conditions. Moreover, the generality of the MFD approach was shown when the node spacing obtained for graphite was used for predicting silicon stress profiles with reasonable accuracy. The effect of reformulated models will be most significant when they are coupled with the macroscopic battery models. Future work is aimed at coupling the efficient solid phase diffusion model with P2D model[1] and reformulated models[23,24] to enable fast and computationally efficient simulation with accuracy for real time control and optimization applications[25–27] for batteries. Real-time simulation of local stress and strain measurement will enable and provide for the use of novel sensors to be included in real-time control and Battery Management System for vehicles.

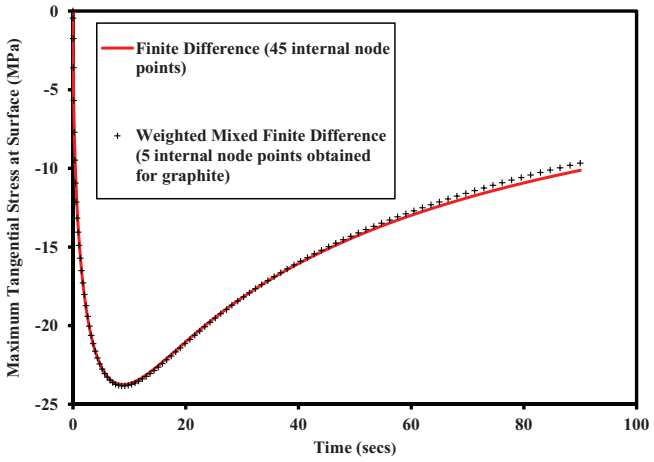

Figure 12. Comparison of maximum tangential stress from the weighted MFD reformulated model and full-order numerical simulation with 45 equally spaced internal node points for charging rate of 1C for silicon using optimal node spacing derived for graphite.

Acknowledgments

The authors are thankful for the financial support by the United States Government, Advanced Research Projects Agency – Energy (ARPA-E), U.S. Department of Energy, under award number DE-AR0000275, and McDonnell Academy Global Energy and Environment Partnership (MAGEEP) at Washington University in St. Louis.

List of Symbols

r	dimensional radial distance within the particle (m)
t	dimensional time (secs)
ξ	dimensionless radial distance within the particle
τ	dimensionless time
$x_{LiS}\ (\xi, \tau)$	dimensionless mole fraction of species *LiS*
$u\ (\xi, \tau)$	dimensionless lattice displacement
$N_{LiS}\ (\xi, \tau)$	dimensionless flux of species *LiS*
$N_S\ (\xi, \tau)$	dimensionless flux of species *S*
$\theta\ (\xi, \tau)$	dimensionless total concentration of binary species
$\sigma_r\ (\xi, \tau)$	dimensionless radial stress
$\sigma_t\ (\xi, \tau)$	dimensionless tangential stress
$\pi\ (\xi, \tau)$	dimensionless pressure
$\chi\ (\tau)$	dimensionless time varying particle radius
ω	fractional expansivity
M_b	dimensionless molar mass ratio of binary species $= \frac{M_{LiS}}{M_S}$
M_i	molar mass of species i, $i = LiS, S$
$x_{\max}$	maximum mole fraction for lithiation
e	dimensionless elastic modulus $= \frac{EM_S}{\rho_s^0 RT(1+\nu)(1-2\nu)}$
E	Young's modulus
ν	Poisson's ratio
R	universal gas constant
T	temperature
ρ_s^0	density of pure unlithiated host
D	dimensionless ratio of diffusive to elastic energy $= \frac{D_{LiS,S}\rho_s{}^0(1+\nu)(1-2\nu)}{R_0{}^2E}$
$D_{LiS,S}$	binary diffusion coefficient
R_0	initial particle radius
I	dimensionless current $= \frac{I_p M_S}{4\pi R_0 F D_{LiS,S}\rho_s{}^0}$
I_p	applied current
F	Faraday constant
N	number of internal node points
N_{var}	number of variables in system
$\overline{N}_{LiS}\ (\xi, \tau)$	dimensionless volume averaged flux of *LiS*
$c_{surf}\ (x, t)$	dimensional surface concentration of *LiS* (mol/m^3)
$j\ (t)$	dimensional local reaction current density (A/m^2)
h_i	optimal node spacing in radial direction

LiS	host material occupied with lithium
S	pure host material

References

1. M. Doyle, T. F. Fuller, and J. Newman, *J. Electrochem. Soc.*, **140**, 1526 (1993).
2. X. Zhang, W. Shyy, and A. Marie Sastry, *J. Electrochem. Soc.*, **154**, A910 (2007).
3. V. Chevrier and J. Dahn, *J. Electrochem. Soc.*, **156**, A454 (2009).
4. J. Christensen and J. Newman, *J Solid State Electr*, **10**, 293 (2006).
5. J. Christensen and J. Newman, *J. Electrochem. Soc.*, **153**, A1019 (2006).
6. S. Renganathan, G. Sikha, S. Santhanagopalan, and R. E. White, *J. Electrochem. Soc.*, **157**, A155 (2010).
7. V. R. Subramanian, J. A. Ritter, and R. E. White, *J. Electrochem. Soc.*, **148**, E444 (2001).
8. V. Ramadesigan, V. Boovaragavan, J. C. Pirkle, and V. R. Subramanian, *J. Electrochem. Soc.*, **157**, A854 (2010).
9. L. R. Petzold, S. L. V. Campbell, and K. E. Brennan, *Numerical Solution of Initial-Value Problems in Differential-Algebraic Equations*, SIAM Press, Philadelphia, PA (1996).
10. V. R. Subramanian, V. D. Diwakar, and D. Tapriyal, *J. Electrochem. Soc.*, **152**, A2002 (2005).
11. C. Wang, W. Gu, and B. Liaw, *J. Electrochem. Soc.*, **145**, 3407 (1998).
12. K. Jagannathan, *J. Electrochem. Soc.*, **156**, A1028 (2009).
13. A. C. Hindmarsh, P. N. Brown, K. E. Grant, S. L. Lee, R. Serban, D. E. Shumaker, and C. S. Woodward, *ACM Trans. Math. Software*, **31**, 363 (2005).
14. J. R. Cash, *Comput. Math. Appl.*, **9**, 645 (1983).
15. E. Hairer and G. Wanner, *Solving Ordinary Differential Equations. II: Stiff and Differential-algebraic Problems*, Springer-Verlag, New York (1981).
16. V. Ramadesigan, P. W. Northrop, S. De, S. Santhanagopalan, R. D. Braatz, and V. R. Subramanian, *J. Electrochem. Soc.*, **159**, R31 (2012).
17. K. Smith and C.-Y. Wang, *J. Power Sources*, **161**, 628 (2006).
18. L. T. Biegler, *Chem. Eng. Process*, **46**, 1043 (2007).
19. S. Kameswaran and L. T. Biegler, *Comput. Chem. Eng.*, **30**, 1560 (2006).
20. Y. Bard, *Nonlinear Parameter Estimation*, Academic Press, New York (1974).
21. W. R. Esposito and C. A. Floudas, *Ind. Eng. Chem. Res.*, **39**, 1291 (2000).
22. A. Flores-Tlacuahuac, S. T. Moreno, and L. T. Biegler, *Ind. Eng. Chem. Res.*, **47**, 2643 (2008).
23. V. R. Subramanian, V. Boovaragavan, V. Ramadesigan, and M. Arabandi, *J. Electrochem. Soc.*, **156**, A260 (2009).
24. P. W. C. Northrop, V. Ramadesigan, S. De, and V. R. Subramanian, *J. Electrochem. Soc.*, **158**, A1461 (2011).
25. S. De, P. W. C. Northrop, V. Ramadesigan, and V. R. Subramanian, *J. Power Sources*, **227**, 161 (2013).
26. S. Golmon, K. Maute, and M. L. Dunn, *Int. J. Numer. Meth. Engng.*, **92**, 475 (2012).
27. N. Xue, W. Du, A. Gupta, W. Shyy, A. M. Sastry, and J. R. R. A. Martins, *J. Electrochem. Soc.*, **160**, A1071 (2013).